Topology in a correlated 2D system: a numerical analysis

Klaus Steiner

August 10, 2017

Abstract

//TODO: write abstract

Introduction

Topological materials are characterized by a nontrivial band structure with interesting properties. Usually the existence of edges is necessary to see the non trivial states in the band structure and allows to distinguish between the trivial bulk states and a number of non trivial edge states which is also known as the bulk-edge correspondence. For a topological insulator this results in a insulating interior bulk states and conducting edge states. The edge states can be identified as singular crossing bands near a symmetry point in the band structure. A fundamental requirement of these topological phases are the existence or absence of symmetries. Depending which symmetry or symmetries and dimension apply to the system it falls into different topological classification with different edge state properties and characteristically topological indices or invariants. These invariants are based on the Berry phase and Berry curvature and should be explained briefly here.

Berry Phase and Berry Curvature

We follow the derivations from [1, p.7 - p.14] here. Consider a system given by the Schrödinger equation

$$\mathcal{H}(\boldsymbol{R}(t))\,|n(\boldsymbol{R}(t)\rangle = i\hbar\frac{d}{dt}\,|n(\boldsymbol{R}(t)\rangle \tag{1.1}$$

for which the normalized eigenstates $|n(\boldsymbol{R})\rangle$ and eigenenergies $E_n(\boldsymbol{R})$ are known. The vector $\boldsymbol{R}$ represents a parameter set i.e position, electric field, magnetic field, strain etc. This system is now moved from time 0 to t adiabatically. The only degree of freedom of the state is the phase depending on time because according to the adiabatic theorem the state $|n(\boldsymbol{R})\rangle$ evolves with the Hamiltonian and only the phase is arbitrary. By adding explicitly a time depending phase $e^{-i\theta(t)}$ to the eigenstate in the Schrödinger equation, applying $\langle n(\boldsymbol{R})|$ from left and solving it for the phase we get

$$\theta(t) = \frac{1}{\hbar}\int_0^t dt' E_n(\boldsymbol{R}(t')) - i\int_0^t dt'\,\langle n(\boldsymbol{R}(t'))|\frac{d}{dt'}|n(\boldsymbol{R}(t'))\rangle\,, \tag{1.2}$$

where the first part is the conventional dynamic phase and the negative of the second part is the Berry phase. The differential operator in the second part can be replaced by gradient operator $\nabla_{\boldsymbol{R}}$ due to the implicit time dependence of the parameter vector $\boldsymbol{R}$. Thus, the Berry phase γ_n can be written as

$$\gamma_n = i\int_0^t dt'\,\langle n(\boldsymbol{R}(t'))|\frac{d}{dt'}|n(\boldsymbol{R}(t'))\rangle = i\int_C d\boldsymbol{R}\,\langle n(\boldsymbol{R})|\nabla_{\boldsymbol{R}}|n(\boldsymbol{R})\rangle\,, \tag{1.3}$$

Now, the γ_n only depends on the curvature C in the parameter space and not explicitly on the time anymore. By defining the vector potential $\mathcal{A}_n(\boldsymbol{R}) \equiv \langle n(\boldsymbol{R})|\nabla_{\boldsymbol{R}}|n(\boldsymbol{R})\rangle$, Equation (1.3) can be rewritten as a curvature integral of a vector potential

$$\gamma_n = \int_C d\boldsymbol{R} \cdot \mathcal{A}_n(\boldsymbol{R}) \tag{1.4}$$

The vector potential $\mathcal{A}_n(\boldsymbol{R})$ is not gauge invariant under the local transformation $|n(\boldsymbol{R})\rangle \to e^{i\chi(\boldsymbol{R})}\,|n(\boldsymbol{R})\rangle$ where $\mathcal{A}_n(\boldsymbol{R})$ transforms as

$$\mathcal{A}_n(\boldsymbol{R}) \to \mathcal{A}_n(\boldsymbol{R}) - \nabla_{\boldsymbol{R}}\chi(\boldsymbol{R}).$$

The function $\chi(\boldsymbol{R})$ is smooth along the curvature C. On the other hand in the case of a closed curvature the Berry phase is indeed gauge invariant modulo 2π. This can be seen by gauge transforming Equation (1.4) along a closed curvature

$$\oint_C d\boldsymbol{R} \cdot \mathcal{A}_n(\boldsymbol{R}) \to \gamma_n - \underbrace{\oint_C d\boldsymbol{R} \cdot \nabla_{\boldsymbol{R}}\chi(\boldsymbol{R})}_{=0}. \tag{1.5}$$

The second term is zero because start and end point of the curvature are the same modulo 2π. If the vector potential is smooth along a closed C, the Stokes' theorem can be used to convert the curvature integral into a surface integral

$$\oint_C d\boldsymbol{R} \cdot \mathcal{A}_n(\boldsymbol{R}) = \int_S d\boldsymbol{S} \cdot \nabla_{\boldsymbol{R}} \times \mathcal{A}_n(\boldsymbol{R}) = \int_S d\boldsymbol{S} \cdot \boldsymbol{\Omega}_n(\boldsymbol{R}) \tag{1.6}$$

where the definition $\boldsymbol{\Omega}_n(\boldsymbol{R}) \equiv \nabla_{\boldsymbol{R}} \times \mathcal{A}_n(\boldsymbol{R})$ is used with $\boldsymbol{\Omega}_n(\boldsymbol{R})$ as the so called Berry curvature of the n-th eigenstate.

Invariants and Symmetries

Based on the previous section we can define an integer number

$$\nu \equiv \frac{1}{2\pi} \int_S d\boldsymbol{S} \cdot \boldsymbol{\Omega}(\boldsymbol{R}) \tag{1.7}$$

which is called Chern number. To see that ν is an integer we can first start evaluating Equation (1.7) on a closed surface $\mathcal{S}$. By applying again Stokes' theorem the integral converts back to an integral over the boundary $\partial\mathcal{S}$ which gives $\nu = 0$ because a closed surface has no boundary. But the previous argument requires that the vector potential $\mathcal{A}(\boldsymbol{R})$ is smooth. Therefore, for a non trivial Chern number a non smooth vector potential is crucial. In fact, a non trivial Chern number manifests that no gauge can be found for which $\mathcal{A}(\boldsymbol{R})$ is smooth. In order to calculate the Chern number for a non smooth vector potential the integral in Equation (1.7) has to be split up in piecewise smooth integrals or patches. Between the patches the vector potentials used in the integrals can be related through gauge transformations and the resulting Chern number is then given by the sum of winding numbers of the gauge transformation along the surface of patches[1, p.31]. As an example the Integer Quantum Hall Effect (IQHE) should be mentioned which was first discovered in 1975. On a 2-dimensional electron gas (i.e in the x-y plane) a

magnetic field perpendicular to the surface is applied. When applying an electric field in x-direction, a current j_y in y-direction can be measured resulting from the conductivity $\sigma_{xy} = \nu e^2/h$ which is quantized and proportional to the Chern number ν. The parameter vector and the surface in Equation (1.7) are the magnetic field and the Brillouin zone (BZ) respectively. In two dimension and periodic boundary condition the surface of the BZ becomes the one of a torus and is therefore closed. Only the non trivial structure of the vector potential gives a non trivial Chern number.

In this report we will focus on the Quantum Spin Hall Effect (QSHE). Compared to the IQHE where the system has no symmetry, for a QSHE breaking the time reversal symmetry is crucial. In detail

$$[\mathcal{H}, \mathcal{T}] = 0 \Rightarrow \mathcal{H} = \mathcal{T}\mathcal{H}\mathcal{T}^{-1} \xrightarrow{\text{F.T}} \mathcal{H}_{-k} = \mathcal{T}\mathcal{H}_k\mathcal{T}^{-1}. \tag{1.8}$$

The time reversal operator $\mathcal{T}$ is an anti-unitary operator and can be composed as $\mathcal{U}\mathcal{K}$ where $\mathcal{U}$ is an unitary operator and $\mathcal{K}$ complex conjugation. In a spin system $\mathcal{U}$ is responsible for flipping the spin and $\mathcal{K}$ changing momentum $\boldsymbol{p}$ to $-\boldsymbol{p}$. Due to the anti-unitary, $\mathcal{T}^2$ can only take the values ± 1. In the case of a Fermionic system invariant under $\mathcal{T}$, $\mathcal{T}^2$ is -1 and the Kramer's theorem holds:

Theorem 1 (Kramer's theorem) *For any eigenstate $|\psi\rangle$ and energy E of a time reversal fermionic system, there exists another state $\mathcal{T}|\psi\rangle$ with the same energy E.*

This degeneracy will play an important role in calculating the $\mathbb{Z}_2$ number, which is the topological invariant for nonmagnetic systems. For an eigenstate $|\boldsymbol{k}\rangle$ the degenerate state is $\mathcal{T}|\boldsymbol{k}\rangle = |-\boldsymbol{k}\rangle$ with different momentum. But for $|\boldsymbol{k} = 0\rangle$ the time reversed state $\mathcal{T}|\boldsymbol{k} = 0\rangle$ is a different state with the same energy and momentum. This i.e also applies for $|\boldsymbol{k} = (0, \pi)\rangle$ in a two dimensional k-grid where $\mathcal{T}|\boldsymbol{k} = (0, \pi)\rangle = |\boldsymbol{k} = (0, -\pi)\rangle$ is the same state. These particular points need to be treated different in the method described in Chapter 2.

The Kramer's theorem is also responsible for the topological protection of the edge state against small perturbation. The well-known Kane-Mele model (see Chapter 2) includes a spin-orbit coupling perturbation where the edge states remain topological.

A more general classification of topological states of matter can be achieved with the ten-fold classification based on three symmetry operation types. For the QSHE we already mentioned the breaking of time reversal symmetry which is in a more general definition a anti-unitary operation. If we also include unitary and chiral operators (unitary operator which anti commutes with the Hamiltonian) we can build upon this a table with the relevant topological invariant for a particular dimension. For a given system with a second quantized Hamiltonian $\hat{\mathcal{H}}$, we can separate it in the following way:

$$\hat{\mathcal{H}} = \hat{\psi}^{\mathrm{T}}\mathcal{H}\hat{\psi} \tag{1.9}$$

where the $\hat{\psi}^{\mathrm{T}}$ and $\hat{\psi}$ are vectors of creation and annihilation operators respectively. This means, that in order to investigate a system, we only have to look at $\mathcal{H}$ and which doesn't necessarily need to be a quantum mechanical system. The system described with Hamiltonian operator $\mathcal{H}$ has to fulfills one or more of the above symmetries criteria.

In the Kane-Mele model perturbation in terms of a spin orbit coupling is included where we still find the topological states.

//TODO: make reference to self energy and what' the purpose of this report (topology with correlation)

Methods

All Results are generated by a program written in C++. The program is based on a older version and was extended to achieve a more flexible configuration and extendability and more important to include self energy. The Hamiltonian used by the program is calculated through the tight binding model (see Appendix A). It takes as program argument a goal, which defines the computation algorithm and the corresponding output it should generate and a configuration file which contains the tight-binding Hamiltonian, grid, k-path, etc. For a more detailed explanation see Appendix B.

Kane-Mele Model

The Kane-Mele model is a honeycomb lattice model which also takes spins into account. It is based on the Haldane model which is a tight binding model having a nearest neighbor and a complex next nearest neighbor hopping. The honeycomb lattice consists of two lattice sites A and B where nearest neighbor hopping t_1 couples A to B and the complex next nearest neighbor hopping operates between same lattice sites (see Figure 2.1). The complex next nearest neighbor hopping comes in the Hamiltonian through a phase ϕ, where from A to B the phase is positive and from B to A negative. The full Hamiltonian in real space is

$$\hat{\mathcal{H}}^{\text{Haldane}} = t_1 \sum_{<i,j>} a_i^\dagger b_j + t_2 \sum_{<<i,j>>} \left(e^{i\phi} a_i^\dagger a_j + e^{-i\phi} b_i^\dagger b_j \right) + M \sum_i \left(a_i^\dagger a_i - b_i^\dagger b_i \right) \tag{2.1}$$

where the first sum is nearest neighbor hopping, the second term the next nearest neighbor hopping (breaks time reversal symmetry) and the last term the on-side energy difference (breaks the inversion symmetry). The $a_i^\dagger / b_i^\dagger$ and a_i / b_i are the creation and annihilation operators for lattice side A/B on grid point i respectively. We extend this Hamiltonian to include spin up and down[5]. For the non interacting part of the Hamiltonian we can simply copy the terms of Equation (2.1) for both spin up and down. Only the next nearest neighbor term looks a bit different.

$$\begin{aligned} \hat{\mathcal{H}}_0^{\text{KM}} = {} & t_1 \sum_{<i,j>,s=\uparrow\downarrow} a_{i,s}^\dagger b_{j,s} + M \sum_{i,s=\uparrow\downarrow} \left(a_{i,s}^\dagger a_{i,s} - b_{i,s}^\dagger b_{i,s} \right) \\ & + t_2 \sum_{<<i,j>>} \left(e^{i\phi} a_{i,\uparrow}^\dagger a_{j,\uparrow} + e^{-i\phi} b_{i,\uparrow}^\dagger b_{j,\uparrow} \right) \\ & + t_2 \sum_{<<i,j>>} \left(e^{-i\phi} a_{i,\downarrow}^\dagger a_{j,\downarrow} + e^{i\phi} b_{i,\downarrow}^\dagger b_{j,\downarrow} \right). \end{aligned} \tag{2.2}$$

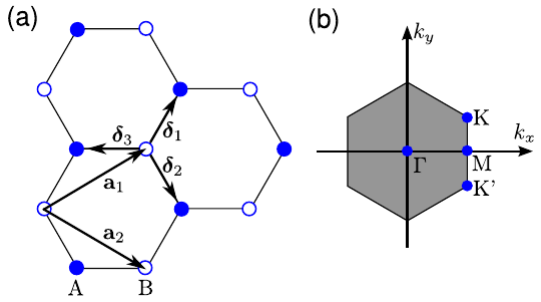

Figure 2.1: (a) Honeycomb lattice[4] with nearest (δ_i) and next nearest neighbors (a_i). (b) The unit cell with the symmetry points Γ, K and K'

Equation (2.2) is invariant under time reversal without giving a proof here. So far, we did not couple electrons with different spins. The goal is to add spin coupling terms while keeping the time reversal symmetry. As long we keep time reversal symmetry the Kramer's theorem hold and we obtain protected edge states visible as crossing bands in the band structure. To see what happens when we add perturbation to the system we can write the Kane-Mele Hamiltonian in the following form

$$\hat{\mathcal{H}}^{\mathrm{KM}} = \begin{pmatrix}\hat{\psi}_\uparrow & \hat{\psi}_\downarrow\end{pmatrix}\begin{pmatrix}\mathcal{H}^{\mathrm{Haldane}}(\phi) & J^\dagger \\ J & \mathcal{H}^{\mathrm{Haldane}}(-\phi)\end{pmatrix}\begin{pmatrix}\hat{\psi}_\uparrow \\ \hat{\psi}_\downarrow\end{pmatrix} \tag{2.3}$$

which is the same separation as in Equation (1.9). The off-diagonal block J is the coupling with the constraint to be anti-symmetric, so $J^{\mathrm{T}} = -J$. Every coupling which flips spins and is anti-symmetric is allowed and fulfills time reversal symmetry. Again, we show no proof here. A possible coupling which satisfies the requirements is the Rashba spin-orbit coupling.

Input Data

For the tight-binding model the input is generated through a DFT + Wannier projection with the Wien2k and Wien2Wannier package.The resulting output after wannierization contains the unit cell structure, neighbor indices, atom indices and the real and imaginary hopping or orbital overlap. The program takes this input and generates a matrix out of it, based on the used boundary conditions. Due to spin-orbit coupling resulting from DFT is very small, we increased it to make it more visible in the band structure. Figure 3.1 and Figure 3.1b shows the band structure of graphene with and without a spin-orbit coupling. The self energy can given as input file, set to a constant value or the analytic form

$$\Sigma(\omega) = \frac{U^2}{4}\frac{\omega - i\delta}{\omega^2 + \delta^2} \tag{2.4}$$

can be used which is the atomic limit for the insulating case. Graphene consists of C atoms in a sp^2 hybridization state. Due to this hybridization there are only two bands in Figure 3.1 π where each band is degenerated by 2. Every C atom

contributes one π electron and occupies the lowest band with one spin up and one spin down electron (the unit cell consists of 2 atoms). In the literature the lower and upper bands are often symmetric compared to the band structure in Figure 3.1. This is because we included also next nearest neighbor hopping in the tight-binding Hamiltonian which makes the band structure look asymmetric.

Spectral Function

//TODO: finish this section and make it better

In order to investigate the behavior of the bands and the topological states when including correlation through self energy we are calculating the spectral function

$$A(\omega, \boldsymbol{k}) = -\frac{1}{\pi}\mathrm{Im}G(\omega, \boldsymbol{k}). \tag{2.5}$$

where $G(\omega, \boldsymbol{k})$ is the Green's function. The program provides three different options for calculation:

1. k-resolved spectral function

$\mathbb{Z}_2$ Calculation

For a QSHE system the Chern number is always zero because in every pair of double degenerate bands both constitutes have opposite Chern number, hence their sum is zero. There is a different characteristic invariant called $\mathbb{Z}_2$, which can only be 0 or 1 depending if it is topological or not. This invariant is connected to the so called pfaffian

$$P(\boldsymbol{k}) = Pf\left\{\langle n(\boldsymbol{k})|\mathcal{T}|m(\boldsymbol{k})\rangle\right\}. \tag{2.6}$$

The absolute value of pfaffian $\left|P(\boldsymbol{k})\right|$ is gauge invariant and only 0 or 1. It turns out that an odd number of zero pfaffians is a topological non trivial system. In order to calculated the $\mathbb{Z}_2$ invariant the space spanned by the eigenstates $|n(\boldsymbol{k})\rangle$ is divided into an even and odd subspace. The even subspace are all eigenstates which follows the constraint

$$\mathcal{T}\,|n(\boldsymbol{k})\rangle = M_{nm}\,|m(\boldsymbol{k})\rangle \tag{2.7}$$

and therefore all k-points satisfying $\mathcal{T}\mathcal{H}(\boldsymbol{k})\mathcal{T}^{-1} = \mathcal{H}(-\boldsymbol{k}) = \mathcal{H}(\boldsymbol{k})$. In graphene the γ and the M points are such time reversal invariant points (TRIM). M_{nm} is a matrix containing only off-diagonal elements. The odd subspace are all states for which

$$B_{mn}(\boldsymbol{k})\mathcal{T}\,|n(\boldsymbol{k})\rangle = |n(-\boldsymbol{k})\rangle \tag{2.8}$$

holds and where $\mathcal{T}\mathcal{H}(\boldsymbol{k})\mathcal{T}^{-1} = \mathcal{H}(-\boldsymbol{k}) = -\mathcal{H}(\boldsymbol{k})$. $B_{nm}(\boldsymbol{k})$ is an unitary matrix called sewing matrix. Kane and Mele showed that there is a binary invariant which can be calculated through

$$I = \frac{1}{2\pi i}\oint_C d\boldsymbol{k}\nabla_{\boldsymbol{k}}\log\left(P(\boldsymbol{k}) + i\delta\right) \tag{2.9}$$

where C is now a curvature around the half of the Brillouin zone and δ a convergence factor. I itself depends on the gauge and the sign of δ but I modulo 2 is indeed invariant. Equation (2.9) counts the number of complex zeros pairs of P. These zeros of the pfaffian are topological invariant. If there is a odd number of zero pfaffian we have a topological system. An alternative form of the $\mathbb{Z}_2$ calculation is

$$I = \frac{1}{2\pi i} \oint_{\partial \mathcal{B}^-} d\boldsymbol{k} \mathcal{A}_i(\boldsymbol{k}) - \int_{\mathcal{B}^-} d\boldsymbol{k} \mathcal{F}_{ij}(\boldsymbol{k}) \tag{2.10}$$

where $\mathcal{B}^-$ denotes know the half BZ and $\mathcal{F}_{ij}(\boldsymbol{k})$ is in analogy to electro dynamics the field strength.

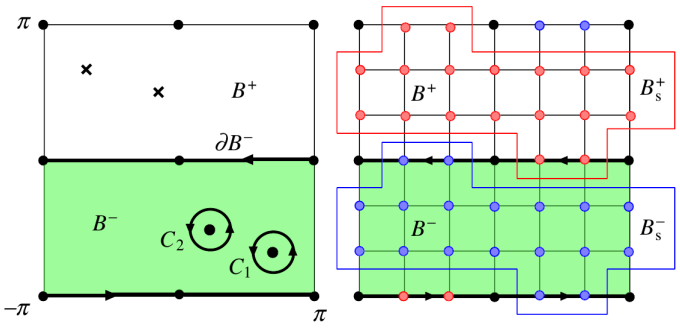

Figure 2.2: The k-space for the $\mathbb{Z}_2$ calculation for the method developed by Fukui and Hatsugai[2]. The space is divided in B^- and B^+ where only B^- is used for calculation. The black dots are the TRIMs, B^-_S are points of the odd space and the black line is the boundary of half the Brillouin zone.

Fukui and Hatsugai[2] build upon this a numerical version for a discrete k-space. $\mathcal{A}_i$ and $\mathcal{F}_{ij}$ are then calculated through a link variable by

$$U_i(\boldsymbol{k}_n) = \frac{\det\left(\psi^\dagger(\boldsymbol{k}_n)\psi(\boldsymbol{k}_n + \hat{i})\right)}{\left|\det\left(\psi^\dagger(\boldsymbol{k}_n)\psi(\boldsymbol{k}_n + \hat{i})\right)\right|} \tag{2.11a}$$

$$\mathcal{A}_i(\boldsymbol{k}_n) = \ln U_i(\boldsymbol{k}_n) \tag{2.11b}$$

$$\mathcal{F}_{ij}(\boldsymbol{k}_n) = \ln\left[U_i(\boldsymbol{k}_n) U_j(\boldsymbol{k}_n + \hat{i}) U_i^{-1}(\boldsymbol{k}_n + \hat{j}) U_j^{-1}(\boldsymbol{k}_n)\right] \tag{2.11c}$$

where U_i is the link variable in direction $\hat{i}$, ψ is a 2×2 matrix spanned by the degenerated eigenvectors for spin up and down, $\boldsymbol{k}_n$ denotes the nth k-point in the grid. For a two dimensional grid $\hat{i}$ and $\hat{j}$ are the two canonical basis vectors in two dimensions respectively. The lattice version of Equation (2.10) for two dimensions is then given by

$$I_{\mathrm{L}} = \frac{1}{2\pi i}\left[\sum_{\boldsymbol{k}_n \epsilon \partial \mathcal{B}^-} \mathcal{A}_1(\boldsymbol{k}_n) - \sum_{\boldsymbol{k}_n \epsilon \mathcal{B}^-} \mathcal{F}_{12}(\boldsymbol{k}_n)\right] \tag{2.12}$$

with the result as an integer and modulo 2 the $\mathbb{Z}_2$ number. The previous calculations can be extended also in 3 dimensions. If we consider the Brillouin zone as a cube we have 6 different surfaces where each of the surface represents a torus due

to periodic boundary conditions. This means we fix on coordinate of the $\boldsymbol{k}$-vector either to 0 or π (to include the TRIMS) and obtain these 6 different possibilities. We follow [2] and denote the invariants of the surfaces as x_0 if $k_x = 0$ or x_π if $k_x = \pi$ and in the same way y_0, y_π, z_0 and z_π. It turns out that in three dimension only 4 $\mathbb{Z}_2$ invariants denoted as $I_0(I_1; I_2; I_3)$ are independent because there are the constraints $x_0 \cdot x_\pi = y_0 \cdot y_\pi = z_0 \cdot z_\pi$. Without any loose of generality we can fix the invariants to $I_0 = x_0 \cdot x_\pi$ and $I_1 = x_\pi$, $I_2 = y_\pi$ and $I_3 = z_\pi$.

Chern Number Calculation

We mention here briefly the calculation of Chern number for the discrete case. It is very similar to the method described in Section 2.4 and taken from [3]. Compared to the $\mathbb{Z}_2$ calculation where the Berry vector potential is non-Abelian because ψ in Equation (2.11) is a 2×2 matrix with U_i as the normalized overlap of the multiplet states, we can define the definition for U_i in Equation (2.11) for a spin-less system as

$$U_i(\boldsymbol{k}_l) = \frac{\langle n(\boldsymbol{k}_l)|n(\boldsymbol{k}_l + \hat{i})\rangle}{\left|\langle n(\boldsymbol{k}_l)|n(\boldsymbol{k}_l + \hat{i})\rangle\right|}. \tag{2.13}$$

In analogy to Section 2.4 the lattice version for Chern number is given by

$$\nu_{\mathrm{L}} = \frac{1}{2\pi i} \sum_l \mathcal{F}_{12}(\boldsymbol{k}_l) \tag{2.14}$$

where $\mathcal{F}_{12}$ is again the field strength and the same definition as in Equation (2.11).

Results

As in the previous chapters mentioned, we are interested in studying the edge states of the topological material under adding correlation through self energy. We are interested in the QSHE based on the Kane-Mele model described in Section 2.1.

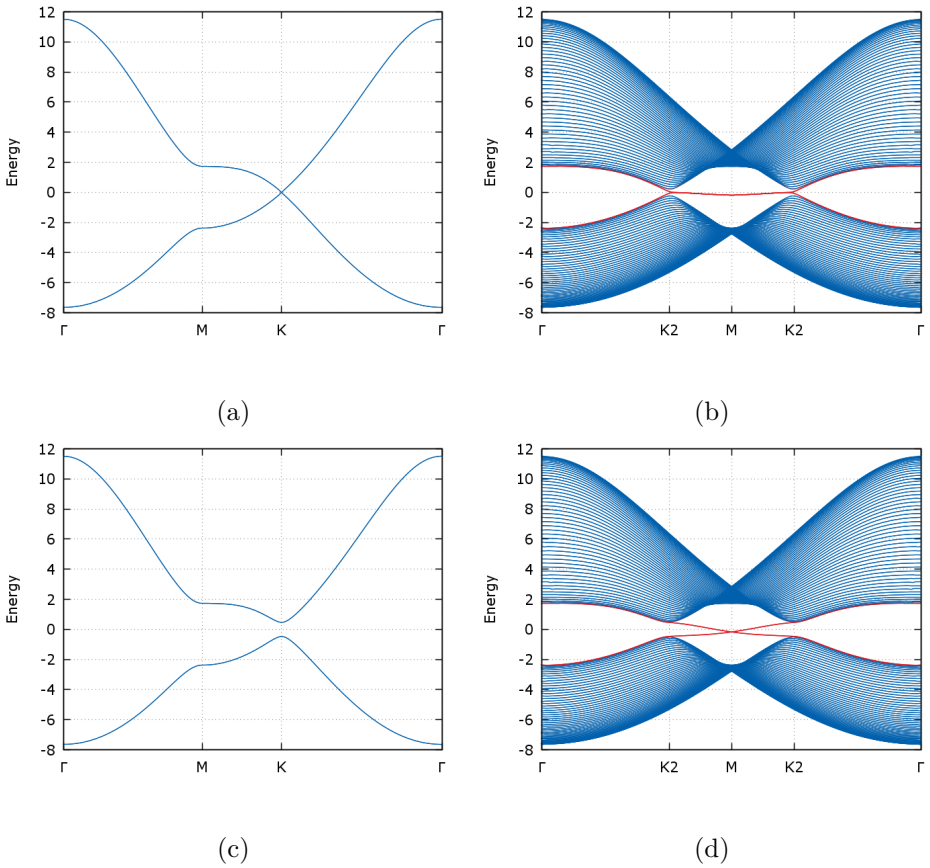

Figure 3.1: Bandstructure calculations for graphene with and without a SOC and periodic and open boundary conditions (BC). The blue lines are the bulk states and the red the edge states. (a) Periodic BC and no SOC, (b) One direction with open BC and no SOC, (c) Periodic BC and SOC, (d) One direction with open BC and SOC

First we verified our model by plotting the band structure of graphene. For the the three dimensional k-path Γ - M - K - Γ in Figure 3.1a and Figure 3.1c we calculated the bandstructure with periodic boundary conditions without and with a spin-coupling (SOC). As expected a gap opens for the case with SOC at the K-point. The next step was to make the bulk finite by applying an open boundary condition in one direction and calculate the bandstructure for the one dimensional k-path Γ - M - Γ in Zig-Zag direction. Figure 3.1b and Figure 3.1d show the results with a bulk consisting of 50 unit cells. Again we included and excluded SOC. The K2-points in this figures is the projection of the K-point in the one dimensional k-path and therefore, the point where the gap opens when adding SOC. The M-point is the important point where the crossing of the edge states occurs. As explained in Section 2.1 the M-point is a TRIM point for which Kramer's theorem holds and the edge states are topological protected. This topological protected can be tested out by adding energy to the edge states and shifting them towards higher energies. If the edge states are shifted over the band gap the next unit cells are taking over as topological states and therefore Kramer's theorem is not violated. This can be seen in Figure 3.2

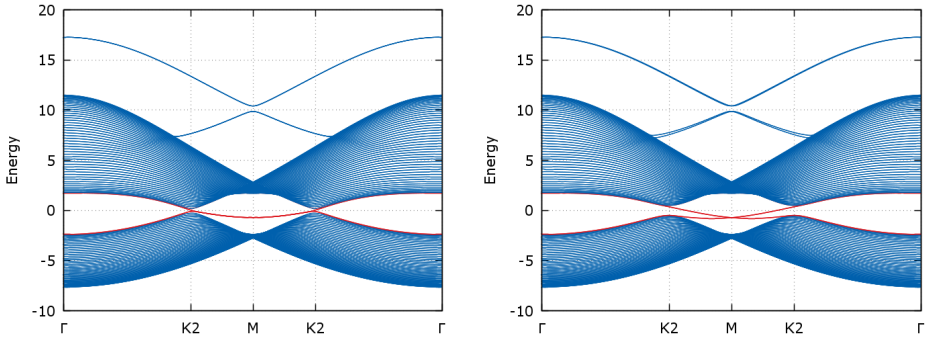

(a) Without SOC (b) With SOC

Figure 3.2: Bandstructure plots when adding real self energy of 10 units at the edge.

Now we include correlation through a self energy $\Sigma(\omega)$ where we distinguish between a metallic and an insulating self energy. In the case of atomic limit, $\Sigma(\omega)$ can be calculated analytical and takes the form in Equation (2.4), so $\propto \frac{1}{\omega}$.

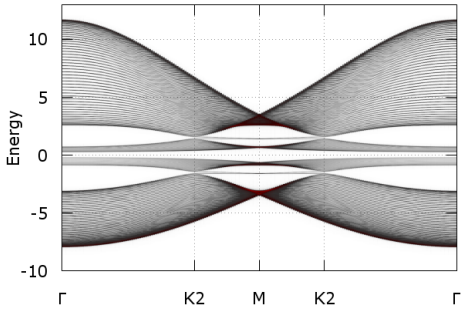

(a) Insulating self energy on edge and bulk with $U = 3$

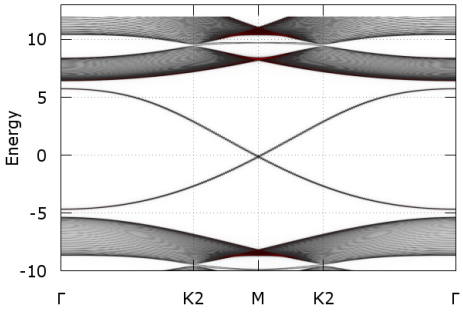

(b) Insulating self energy in bulk with $U = 19$ and metallic self energy on edge.

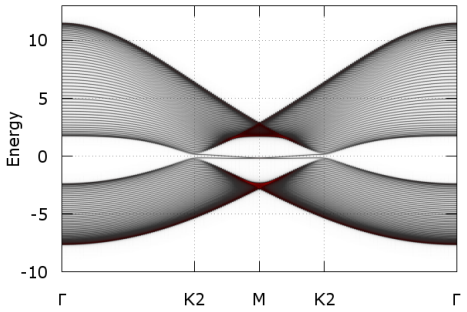

(c) Metallic self energy in bulk and on edge.

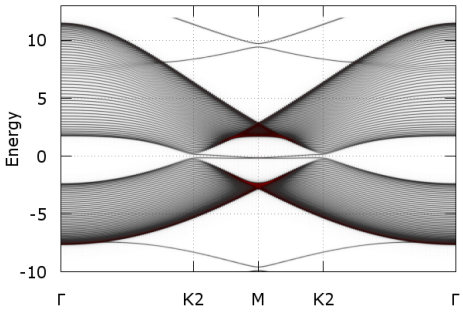

(d) Metallic self energy in bulk and insulating self energy with $U = 19$ on edge.

Figure 3.3: Spectral function plots for different analytical self energies in bulk and on edge.

Figure 3.3 to Figure 3.3c show the spectral function plots with different U values. For the case with insulating bulk and edge an increasing U separates the lower and upper Hubbard bands. The two valence bands around the Fermi energy are getting thinner with lower U due to a pole at zero energy which forces the squeezing of the bands. For metallic self energy on edge, insulating self energy in bulk and U bigger than the band gap, the crossing bands in Figure 3.3a are resulting from a one dimensional chain created by the boundary conditions. Except of the one dimensional chain bands the plot is the same as Figure 3.3 only with higher U. In the case of insulating edge and metallic bulk the resulting spectral function plot is Figure 3.3c. As it can be seen, the insulating self energy shifts out the edge states but the system remains topological.

Conclusion

Tight Binding Model

Program

Bibliography

[1] B.A. Bernevig and T.L. Hughes. *Topological Insulators and Topological Superconductors*. Princeton University Press, 2013. ISBN: 9780691151755. URL: https://books.google.at/books?id=wOn7JHSSxrsC.

[2] Takahiro Fukui and Yasuhiro Hatsugai. "Quantum Spin Hall Effect in Three Dimensional Materials: Lattice Computation of Z2 Topological Invariants and Its Application to Bi and Sb". In: *Journal of the Physical Society of Japan* 76.5 (2007), p. 053702. DOI: 10.1143/JPSJ.76.053702. eprint: http://dx.doi.org/10.1143/JPSJ.76.053702. URL: http://dx.doi.org/10.1143/JPSJ.76.053702.

[3] Takahiro Fukui, Yasuhiro Hatsugai, and Hiroshi Suzuki. "Chern Numbers in Discretized Brillouin Zone: Efficient Method of Computing (Spin) Hall Conductances". In: *Journal of the Physical Society of Japan* 74.6 (2005), pp. 1674–1677. DOI: 10.1143/JPSJ.74.1674. eprint: http://dx.doi.org/10.1143/JPSJ.74.1674. URL: http://dx.doi.org/10.1143/JPSJ.74.1674.

[4] M Hohenadler and F F Assaad. "Correlation effects in two-dimensional topological insulators". In: *Journal of Physics: Condensed Matter* 25.14 (2013), p. 143201. URL: http://stacks.iop.org/0953-8984/25/i=14/a=143201.

[5] C. L. Kane and E. J. Mele. "Z_2". In: *Phys. Rev. Lett.* 95 (14 2005), p. 146802. DOI: 10.1103/PhysRevLett.95.146802. URL: https://link.aps.org/doi/10.1103/PhysRevLett.95.146802.